Direct Observation of Polymer Dynamics: Mobility Comparison between Central and End Section Chain Segments

K. A. Welp and R. P. Wool*

Department of Chemical Engineering, University of Delaware, Newark, Delaware 19716

G. Agrawal[†]

Department of Materials Science & Engineering, University of Illinois, Urbana, Illinois 61801

S. K. Satija

Center for Neutron Research, National Institute of Standards and Technology, Gaithersburg, Maryland 20899

S. Pispas[‡] **and J. Mays**

Department of Chemistry, University of Alabama at Birmingham, Birmingham, Alabama 35294

Received February 11, 1999; Revised Manuscript Received June 1, 1999

ABSTRACT: In this work the motions of chain segments in either the central 50% of a polymer or in the two end sections (25% each) were probed. Motions of the central (or end) section were measured using bilayer welding samples of deuterium-labeled polymers. Symmetric triblock poly(styrene) (HDH) was paired with fully deuterated or fully protonated poly(styrene) of nearly equal molecular weight. Changes in the deuterium profile of a given pair were directly linked to the motions of a given section of the chain. The behavior of the deuterium depth profiles was monitored using specular neutron reflectivity (SNR). Rouse and reptation model predictions for the behavior of chain segments in the end and center sections were developed using computer simulations and minor chain reptation calculations. These dynamics models are representative of two broad classes of dynamics theories: tubeless (Rouse) and tubed (reptation). These experiments were thus designed to discriminate between tubeless and tubed dynamics. Segments in the central sections showed a distinct lag in crossing the interface, while segments in the end sections crossed the interface continuously. This chain centers' lag behavior is a distinctive signature of the reptation model and is not predicted by tubeless models. These experiments offer a simple and direct observation of the highly anisotropic tube motions of entangled polymer melt chains, providing strong support for the use of reptation to describe dynamics of melt polymers at the weld interface.

1. Introduction

Understanding the dynamics of polymer chains at interfaces is critical to many applications, including welding, fracture strength development, composite lamination, particle sintering, coatings, and adhesion.[1] Much work has been done on steady-state or long-time diffusion in polymers,[2−5] but it is the short-time interdiffusion at a polymer−polymer, or weld, interface that determines the critical properties of the interface. Motions resulting in interpenetration on the order of the radius of gyration, R_g, e.g. about 175 Å for a 400K poly(styrene) sample, define short time.

Through the use of specially labeled polymer chains, the short-range dynamics of linear polymers near the polymer weld interface can be monitored.[6−9] Triblock polymer chains have been synthesized where the labeling is symmetric about the chain center, and the deuterium content was about 50%. The chain architecture for a protonated−deuterated−protonated triblock (HDH) is shown in Figure 1.

Previously we have used bilayers of oppositely labeled triblock poly(styrene)s, HDH/DHD, to investigate the dynamics of polymer chains during welding.[1,6−9] The nature of the opposing labeling architecture creates enrichment (HDH side) or depletion (DHD side) of deuterium during welding at early times, due to differing mobility of segments in the end versus those in the center sections. These enrichment/depletion signatures, and the experiment that produces it, have been called the "ripple". We have seen ripple profiles in all HDH/DHD samples using entangled polymers. While all polymer dynamics models predict concentration ripples, the details of the amplitude and distance from the weld interface are unique to each dynamics model. In this way, the ripple experiment provides a fingerprint of the dynamics. That work supports reptation as the correct dynamics model to describe the interdiffusion of polymer chains.[6,9]

The reptation model developed concurrently by de-Gennes[10] and Doi and Edwards[11] predicts that polymer chains move under a highly anisotropic friction due to entanglements with their neighboring chains. This anisotropy manifests itself as a snakelike motion where the central section follows end sections across the weld interface during interdiffusion. The diffusion distance of reptating ends across the interface is a smooth increasing function of time, while the diffusion of center sections shows a lag or delay. Tubeless models, such as

* Corresponding author.
[†] Present address: PPG Industries, Inc., Allison Park, PA 15101.
[‡] Present address: Department of Chemistry, University of Athens, 15771 Greece.
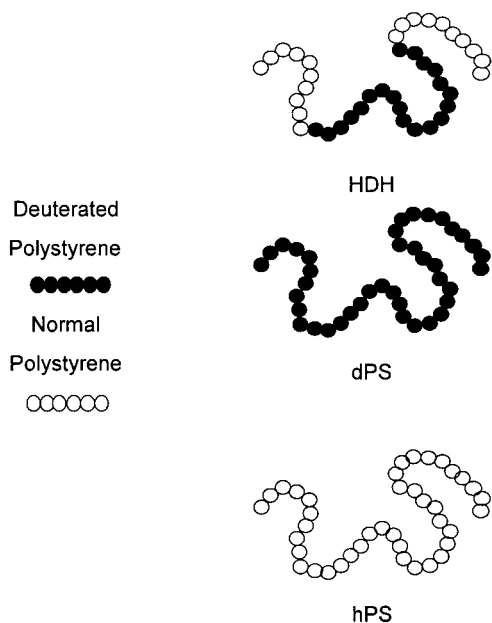
Figure 1. Poly(styrene) chains used in this work. HDH chains have deuterated segments in the center of the chain, 50% of total length, while the remaining segments (in the end sections) were protonated. hPS and dPS chains were fully protonated or deuterated, respectively.

Table 1. Properties of Poly(styrene) Materials Used in This Work[a]

sample	M_w	M_w/M_n	% D
HDH	464 000	1.04	55
dPS	550 000	1.05	100
hPS	400 000	1.06	0

[a] M_w is the weight-average molecular weight, M_n is the number-average molecular weight, and % D is the mole percent of perdeuterated segments.

polymer mode−mode coupling (PMC)[12] and Rouse[13] dynamics, predict that both polymer centers and ends will cross the interface at all times due to their isotropic friction coefficient. No delay or lag in the motion of centers across the interface is expected, although the relative velocity of the ends is greater. The aim of this work was to observe directly and independently the mobility of chain center and end sections, to determine which of these sharply differing predictions best describes interdiffusion at the weld interface.

In this work we directly observe the motion of either end sections of polymer chains or center sections of identical polymer chains during interdiffusion using a pair of polymer bilayer samples (Figure 2). The first sample was designed to monitor only motion of segments in the end sections of a polymer chain across the interface. Bilayers of HDH and dPS polymers (Figure 2a) were used to isolate end segment motions. The segments in the center sections of both polymers were deuterated and thus identical. In contrast, segments from end sections were different: one deuterated and the other protonated. This labeling produced a deuterium concentration profile perpendicular to the interface, or depth profile, that was initially a sharp step function. When end sections cross the interface during interdiffusion, the step profile will broaden due to the exchange of D for H, or H for D, across the interface. The even exchange of segments is dictated by the matched molecular weights of the two polymers (Table 1), which requires equal but opposite flux during interdiffusion. This process and the resulting broadening of the depth profile are demonstrated in Figure 2a. The deuterium depth profile of an "ends" sample (HDH/dPS) was then sensitive only to motions of segments from the end section of the chains across the interface.

The second sample was designed to probe the mobility of segments from the central sections of polymer chains across the polymer−polymer interface during interdiffusion. The "centers" experiment used bilayer samples

of HDH and hPS polymers (Figure 2b). Here the labeling of segments in the end sections of both polymers was identical. Interdiffusion of segments from the end sections does *not* alter the initial step depth profile, since the end segments crossing the interface involves a simple H for H exchange (Figure 2b). Conversely, the segments in the central sections were oppositely labeled. The movement of central sections across the interface is then the only process that results in broadening of the initial step deuterium depth profile, shown in the third panel of Figure 2b. The combination of ends (HDH/dPS) and centers (HDH/hPS) experiments allows the mobility of segments in the end and central sections of polymer chains to be directly probed, as demonstrated herein.

2. Computer Simulations and Calculations

2.1. Characterization of Chain Segment Mobility. Interface broadening was characterized by the average monomer interpenetration distance, $\langle X(t) \rangle$, written

$$\langle X(t) \rangle = \frac{\int_0^\infty x C(x,t)\,\mathrm{d}x}{\int_0^\infty C(x,t)\,\mathrm{d}x} \quad (1)$$

Here x is depth, t is welding time, and $C(x,t)$ is the deuterium concentration profile. In a welding experiment, $\langle X \rangle$ is the average distance from the interface of segments that have migrated across the weld interface via diffusion. This polymer interpenetration is responsible for weld strength development when polymers are welded.[1] For HDH/dPS samples, the diffusion of the end section of a triblock chain changes the deuterium concentration profile and thus alters $\langle X(t) \rangle_E$, the average interdiffusion depth of segments in the end section of the chain. Conversely, in the HDH/hPS architecture, the diffusion of chain center sections changes the deuterium concentration profile and hence alters $\langle X(t) \rangle_C$, the average interdiffusion depth of segments in the center section of the chain. Both of the $\langle X(t) \rangle$ quantities discussed can be measured for different dynamics models using computer simulation, recording the label of a segment (end or center) along with its spatial coordinates.

2.2. Rouse Dynamics. An off-lattice Monte Carlo simulation using the bead−spring model was used to simulate Rouse dynamics. The initial conformations were constructed using a reflecting boundary condition at the interface. A Monte Carlo algorithm was used to determine acceptance of segment moves, where a move consists of displacing a randomly selected bead along a random vector (white noise). The acceptance of a move was weighted with a probability function proportional to the exponent of the spring elastic energy difference between the new and prior configurations. The time axis
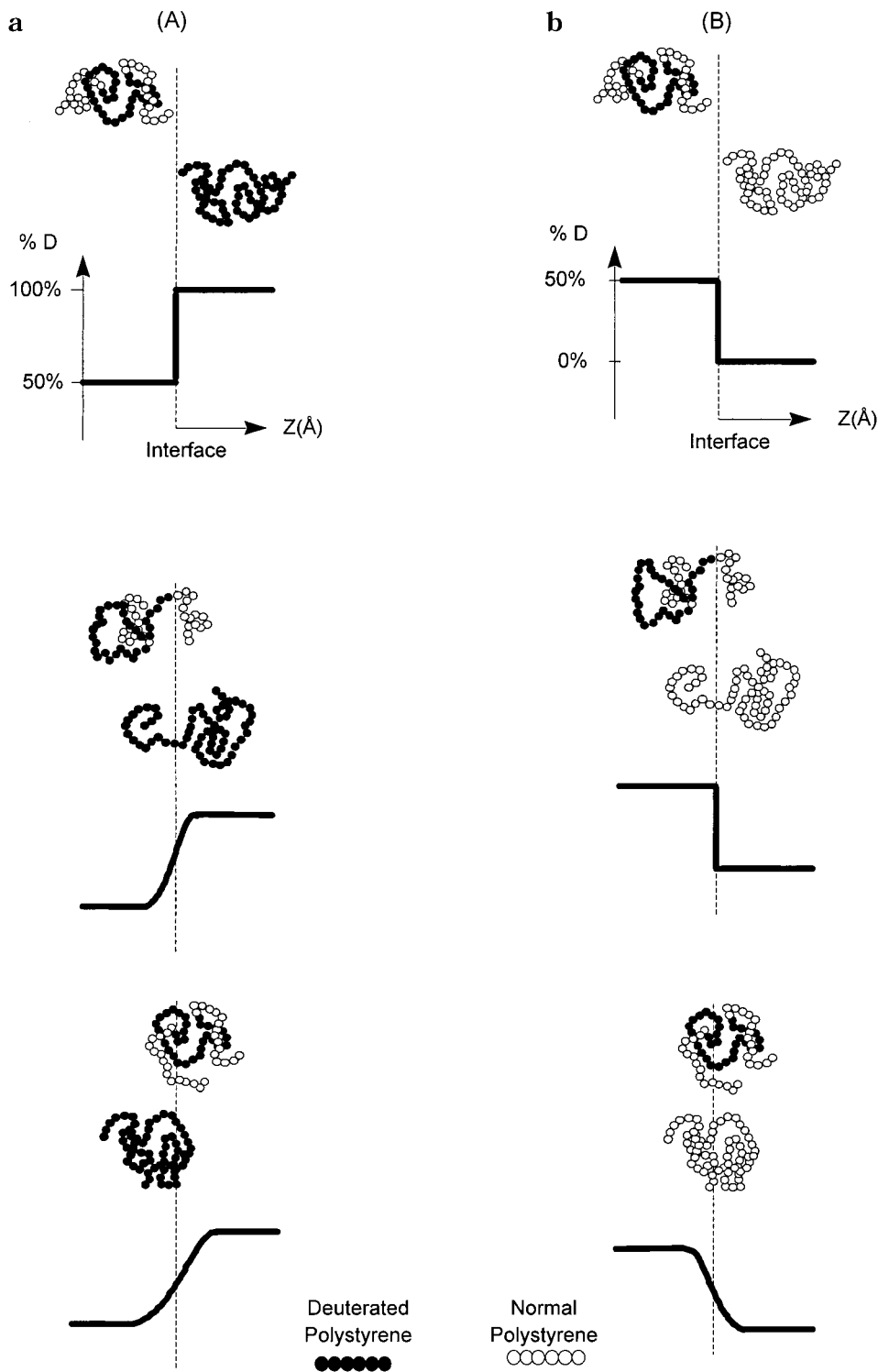
Figure 2. Interdiffusion behavior, and resulting deuterium depth profiles, of chains experiencing highly anisotropic friction for (a) HDH/dPS, or ends, and (b) HDH/hPS, or centers samples. Welding time increases from top to bottom. The predicted lag in mobility of centers is observable via the delay in interfacial broadening for the centers case under snakelike dynamics, top to middle.

scales with the number of moves attempted, and bead motions as a function of time were examined. The single chain simulation was repeated many times to generate ensemble average properties.

To confirm the ability of the algorithm to simulate Rouse dynamics, the ensemble average bulk properties were compared to the predictions of the Rouse model. The end-to-end vector orientation relaxation function $(f(t) = \langle \mathbf{R}(t) - \mathbf{R}(0) \rangle)$ behaved as $f(t) \sim \exp(-t/\tau)$. The

relaxation time (τ) versus chain length (N) behaved as

$$\tau \approx 9.7 N^2 \qquad (2)$$

while the center-of-mass diffusion coefficient (D) versus chain length behaved as

$$D \approx 0.008 N^{-1} \qquad (3)$$

These results were in agreement with the predictions of the Rouse dynamics theory.[13]

This algorithm can then be used to predict the behavior of ends and centers samples undergoing Rouse dynamics. A center or end label was added to the segment coordinate matrix such that this matrix included both the location of a segment in the chain (end or center) and its spatial position. This allowed predictions of end (or center) mobility under Rouse dynamics from computer simulations. The number of end/center segments at any distance d from the interface was written at any time t as $N_E(d,t)/N_C(d,t)$. Calculating $N_E(x,t)$, where x includes all d at or beyond the interface, provided a concentration profile of end segments that have crossed the interface. The average monomer interpenetration depth at time t ($\langle X(t) \rangle$) was then calculated using eq 1 and these $N(x,t)$ segment concentration profiles.

2.3. Reptation Dynamics. Random walk chains of length N were assembled on a two-dimensional lattice with a reflecting boundary condition at the interface ($x = 0$). Chains were constructed at varying initial distances from the interface, resulting in a uniform density profile of both chain segments and chain ends. This assured that surface-sensitive properties such as average monomer interpenetration depth were not altered by anomalous enrichment of either segments or ends to the surface by the chain construction algorithm. In separate experiments, we have shown that chain ends do not segregate from depths greater than a tube diameter, in agreement with previous reports.[14-16] Therefore, chain end segregation was not important in these experiments. The simulated chain static properties agreed with Gaussian statistics expected for melt chains: mean-square radius of gyration with chain length $R_g^2 \sim N^1$ and ratio of mean-square end-to-end distance to mean-square radius of gyration $R^2/R_g^2 = 6$.

Chain motion was induced by the random selection of a chain end segment, followed by random selection of an adjacent lattice position. A new segment was then added at this lattice site, and the last segment from the other end of the chain was deleted, maintaining constant chain length. Each segment also had a label (end or center), and these labels were adjusted after each move to maintain the 25−50−25 HDH architecture shown in Figure 1. The chain center section thus moves back and forth along the original chain contour in the characteristic snakelike motion, while the chain ends exhibit Brownian motion as they explore new lattice sites. This experiment was repeated for all constructed chains to produce ensemble average results. The reptation time, τ, was obtained by measuring the fraction of the segments remaining within the initial tube, $\phi(t)$, as a function of time:

$$\phi(t) = 1 - \frac{4}{\pi^{3/2}} \left(\frac{t}{\tau} \right)^{1/2} \tag{4}$$

It is evident from eq 4 that, at $t = \tau$, $\phi(t)$ is about 0.28. The relaxation time determined in this manner behaves as $\tau \sim N^3$, consistent with the reptation model. The self-diffusion coefficient, D, mean-square center-of-mass displacement, $\langle R_{cm}^2 \rangle$, and mean-square segment displacement, $\langle R^2 \rangle$, predicted by these simulations were also consistent with reptation predictions and behaved as

$$D \sim M^{-2}$$

$$\langle R_{cm}^2 \rangle \sim t^1$$

$$\langle R^2 \rangle \sim t^{1/2} \quad \text{for } t < \tau$$

$$\langle R^2 \rangle \sim t^1 \quad \text{for } t > \tau \tag{5}$$

The average interpenetration depth for the entire chain was calculated as the ratio of the sum of the positions of all segments that have crossed the interface and the total number of segments that have crossed the interface, N_c,

$$\langle X(t) \rangle = \frac{\sum_{i=0}^{\infty} x_i}{N_c} \quad \text{for } x_i > 0 \tag{6}$$

where x_i is the position of segment i and the interface is at $x = 0$. Limiting the summation and N_c terms in eq 6 to segments labeled as either end or center allows prediction of end and center average interpenetration depths ($\langle X \rangle_E$ and $\langle X \rangle_C$). The agreement of these simulations with the scaling laws of the reptation dynamics model of deGennes[10] and Doi−Edwards,[11] eq 5, validates the ability of the algorithm to generate reptation model predictions for the mobility of polymer chain end and center sections across the polymer−polymer interface.

2.4. Minor Chain Reptation Calculations. The minor chain reptation model calculates the portions of a chain that have escaped the initial tube due to snakelike motions for time t.[1,17,18] These escaped portions are called minor chains (two per polymer molecule), and their length increases with time. The time dependence of the minor chain length, n, is described by

$$n(t) = 2N \sqrt{\frac{t}{\pi^3 \tau}} \tag{7}$$

where N is the chain length, t the welding time, and τ the relaxation time.[17] The model was modified slightly here by the use of a three-dimensional Gaussian coil for each minor chain in the calculation of the monomer concentration functions.[19] The analytical form for the monomer concentration profile is

$$C(x,t) = \frac{\rho}{M} \int_{n_A(t)}^{n_B(t)} \text{erfc} \sqrt{\frac{3x^2}{2sb^2}} \, ds \tag{8}$$

where ρ is the density of the polymer melt, M the molecular weight, x the distance from the interface, and s the coordinate along the minor chain contour. The integration limits $n_A(t)$ and $n_B(t)$ depend on time via eq 7 and the portion of the chain for which the concentration profile was to be calculated (entire chain, end section, or center section). The selection criteria for n_A and n_B are summarized in Table 2. The integration limits, n_A and n_B, also depend on the length of the end-labeled sections of the chain. Therefore, Table 2 reflects the 25−50−25 (percent end−center−end) symmetric architecture used herein. Combining eq 8 and Table 2, concentration profiles of segments in the end or center section of a polymer chain were calculated. These

Table 2. Criteria for Selection of Integration Limits, n_A and n_B, in Eq 8 Used To Calculate Minor Chain Reptation Concentration Profiles for the Whole Chain, End Sections, and Central Section[a]

integration limits	whole chain	chain ends		chain centers	
		$n(t) < N/4$	$n(t) > N/4$	$n(t) < N/4$	$n(t) > N/4$
n_A	0	0	$n(t) - N/4$	0	0
n_B	$n(t)$	$n(t)$	$n(t)$	0	$n(t) - N/4$

[a] $n(t)$ is the minor chain length, given by eq 7, and n is the total length of the chain.

concentration profiles generated the desired minor chain reptation $\langle X(t) \rangle_E$ and $\langle X(t) \rangle_C$ predictions when substituted into eq 1.

3. Experimental Techniques

To probe the mobility of end and center sections of polymer chains in the amorphous melt, two welding configurations, shown in Figure 2, were used. These welding pairs, HDH/dPS and HDH/hPS (Table 1), were prepared by bringing two polymer films into intimate contact in the glassy state. Interdiffusion between the polymer layers occurs only during controlled welding above the glass transition temperature. Differences in labeling (H vs D) create contrast between the layers from specific sections of the polymer chains, as shown via concentration profiles in Figure 2.

These experiments require the measurement of deuterium depth profiles at buried interfaces in polymeric samples. A technique capable of penetrating through the polymer to the buried interface and providing good depth resolution at that interface was required to obtain experimental data that could be compared to model predictions in a meaningful way. Specular neutron reflectivity (SNR) is a very high-resolution technique (~10 Å) capable of penetrating several hundred angstroms. The contrast between protonated and deuterated poly(styrene) is very high in neutron experiments, and thus the technique is highly sensitive to changes in the deuterium depth profile.

3.1. Sample Preparation. Triblock poly(styrenes) (HDH) were prepared using "living" anionic polymerization initiated with *sec*-butyllithium.[9] Sequential addition of hydrogenous and then deuterated styrene monomers produced symmetric diblock polymers. These diblocks were then coupled at the active deuterated chain ends by dichlorodimethylsilane. Solvent/nonsolvent (toluene/methanol) fractionation was used to remove residual diblock. Homopolymer hPS was obtained from Pressure Chemical and dPS from Polymer Laboratories. Properties of the poly(styrene) materials used in this work are given in Table 1.

Polymer bilayers were prepared on single-crystal silicon wafers (4 in. diameter, polished one side) by spin coating (Headway Research PM101DT-R790). All steps were conducted in a clean room environment to prevent surface contamination. Si wafers were first degreased with acetone and methanol and subsequently etched in a hydrofluoric acid solution to a completely hydrophobic surface (SiH$_x$). They were rinsed in 18 MΩ·cm water and spun dry with toluene. HDH polymer was dissolved in toluene and filtered three times through a 0.8 μm pore filter (Millipore). This solution was then spun onto the substrate. Concentrations of polymer solution and spin speed were selected to produce films ~800 Å thick. This thickness was greater than $4R_g$ for 400K poly(styrene), eliminating confined film or polymer–substrate interaction effects on interdiffusion. HDH (on Si) films were then annealed at 120 °C under vacuum for 12 h.

Homopolymer (hPS or dPS) layers were prepared by spin coating onto cleaned glass plates and added to the sample by floating the films onto a pool of clean (18 MΩ·cm) water and capturing them on the HDH-coated substrate. A freshwater bath was used for each film to prevent contamination. Si HDH/(hPS or dPS) samples were then dried in a vacuum for 24 h at 70 °C to remove residual water.

3.2. Welding. HDH/(dPS or hPS) bilayers were subjected to welding at temperatures of 120–128.5 °C for differing times to produce samples with a range of interdiffusion conditions. The longest relaxation time of 400K PS at 120 °C, τ, was estimated to be 123.2 h using

$$\tau = \frac{R^2}{3\pi^2 D} \quad (9)$$

where the root-mean-square end-to-end distance, R, is 427 Å, and D is the center-of-mass diffusion coefficient. The temperature dependence of D was estimated using the Vogel–Fulcher relationship,

$$\log\left(\frac{D}{T}\right) = A - \frac{B}{T - T_{inf}} \quad (10)$$

where the parameters $A = -9.789$ and $B = 710$ were estimated from bulk diffusion data of 255K PS and $T_{inf} = 322$ K for PS.[2] The diffusion coefficient of 255K PS at the welding temperature of interest, calculated using eq 10, was next scaled to the molecular weight of these samples (400K) using the well-known scaling law for entangled polymers, $D \sim M^{-2}$. The resulting diffusion coefficient, at the molecular weight and welding temperature used, was used in eq 9 to estimate relaxation times for these polymers.

Welding was performed at several temperatures in order to capture widely spaced phenomena within a reasonable experimental time frame. The recorded welding times at all temperatures were reduced to times at a basis temperature of 120 °C by dividing by the WLF shift factor at welding temperature T, a_T, calculated from

$$\log a_T = -9.06 \frac{T - 120}{69.8 + T - 120} \quad (11)$$

where parameters for PS from Tassin et al. are shown.[20] Experimental features can then be plotted as a function of welding times at 120 °C, independent of the actual welding temperature.

3.3. Specular Neutron Reflectivity, SNR. Specular neutron reflectivity (SNR) experiments were performed on the NG-7 spectrometer at the NIST Center for Neutron Research (NCNR). Neutron reflectivity involves directing a collimated beam of neutrons onto a surface at a glancing angle (<3°) and measuring the ratio of the reflected to incident intensity as a function of neutron momentum perpendicular to the interface, q_z, given by

$$q_z = (4\pi/\lambda) \sin \theta \quad (12)$$

where λ is the wavelength of the neutron beam and θ the angle of incidence. Reflection occurs due to differences in the scattering length density, ρ_b, analogous to the index of refraction in the reflection of visible light. The Si/HDH/hPS(dPS) samples have high contrast as evidenced by the ρ_b values for the species in the system: 6.3×10^{-6} Å^{-2} for deuterated poly(styrene), 1.4×10^{-6} Å^{-2} for protonated poly(styrene), and 2.1×10^{-6} Å^{-2} for silicon. Detailed treatments of reflectivity appear in the literature.[21-25]

Model fitting was required to extract concentration depth profiles from SNR data due to their lack of phase information, the inverse scattering problem. The model depth profiles used to fit these data have two layer compositions, three interface widths (air–polymer, polymer–polymer, and substrate–polymer), and two layer thickness values as fitting parameters. Fitting was performed using SERF, which performs necessary reflectivity fitting calculations within a spreadsheet.[26] SERF combines simultaneous numerical and graphical data representation with command-free recalculation, improving both the input model flexibility and overall speed of the fitting procedure. Supplementary information, including film thickness (ellipsometry) and interfacial roughness (X-ray reflectivity), was obtained and included in the initial model and used to
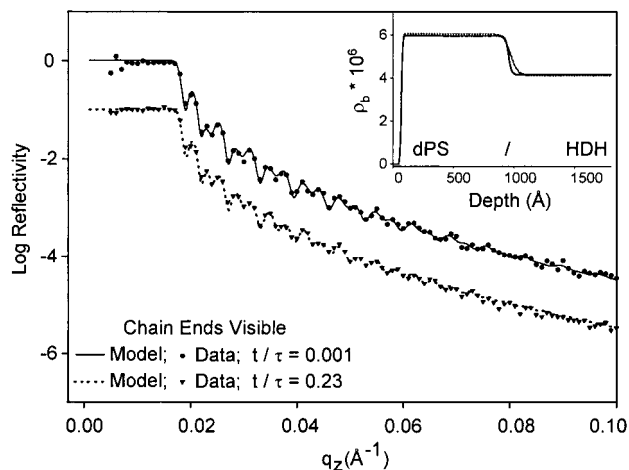
Figure 3. Log reflectivity vs q_z (Å^{-1}) for early, 0.001τ, and intermediate, 0.23τ, welding times for HDH/dPS, or the ends case. Symbols represent experimental data, and curves represent model fits calculated from scattering length density (ρ_b) depth profiles using SERF and shown at inset.
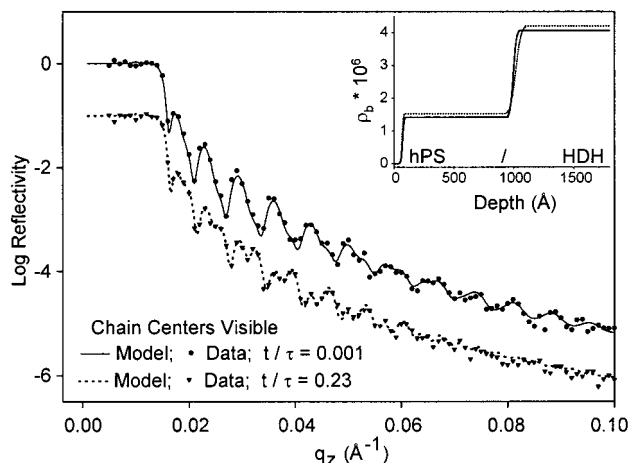

Figure 4. Log reflectivity vs q_z (Å^{-1}) for early, 0.001τ, and intermediate, 0.23τ, welding times for HDH/hPS, or the centers case. Symbols represent experimental data, and curves represent model fits calculated from scattering length density (ρ_b) depth profiles using SERF and shown at inset.

define constraints on the depth profile model parameters. These physical constraints, along with global parameter searches using randomly selected initial points for minimization (Sobol sequence), allow the authors to conclude that the fits to these data are consistent with the real sample profile and represent the global minimum in the parameter space. Figures 3 and 4 illustrate typical reflectivity data and model fits obtained using SERF for dPS/HDH/Si and hPS/HDH/Si samples, respectively. The inset plots of Figures 3 and 4 show the scattering length density (ρ_b) versus depth profiles used to calculate the model reflectivity, shown by curves, along with the reflectivity data, symbols, in Figures 3 and 4. The scattering length density at a given depth is directly proportional to the deuterium concentration at that depth. Thus, SNR, with the help of SERF, provides high-resolution deuterium depth profiles from polymer welding samples.

4. Results and Discussion

4.1. Computer Simulation and Calculation Results. 4.1.1 Rouse Simulations. Simulation predictions of average monomer interpenetration depth for chain ends, $\langle X \rangle_E$, and chain centers, $\langle X \rangle_C$, versus welding time for Rouse dynamics are shown in Figure 5. The
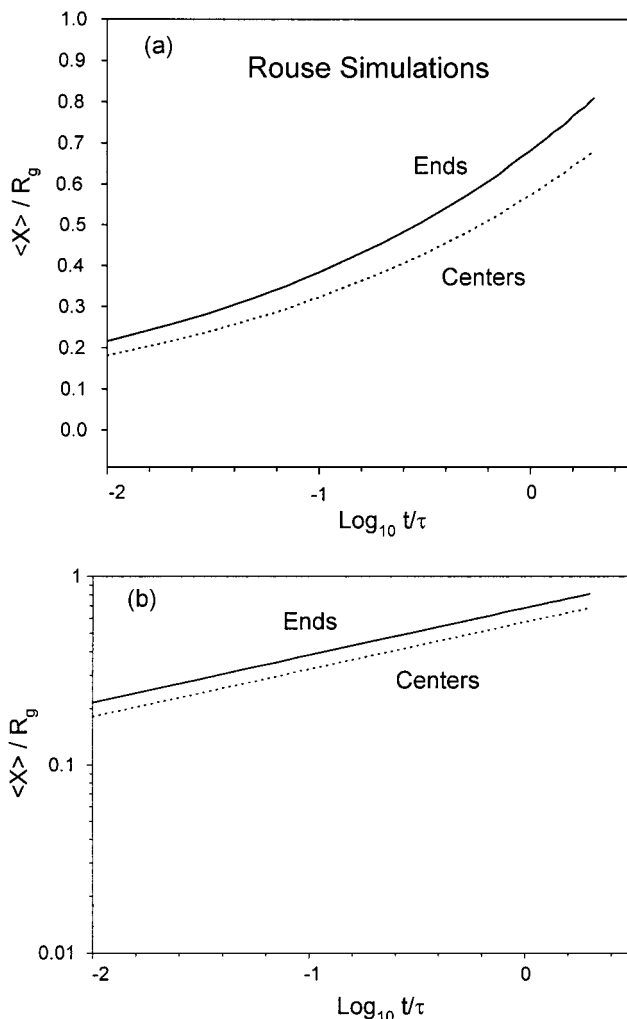
Figure 5. Rouse predictions for average monomer interpenetration depth vs welding time for segments in the end ($\langle X \rangle_E$, solid curve) and center sections ($\langle X \rangle_C$, dotted curve) from computer simulations. Data are plotted on (a) linear−log axes and (b) log−log axes. In (a), $\langle X \rangle_E$ and $\langle X \rangle_C$ both increase continuously, and in (b), both ends and centers show a slope of $^1/_4$ at all $t < \tau$.

$\langle X \rangle$ values were normalized with the radius of gyration (R_g) and welding times with the longest relaxation time for Rouse chains (τ). Both the chain centers and ends crossed the interface continuously on a linear−log plot (Figure 5a). Figure 5b plots these same data on log−log scales to determine time scaling exponents of $\langle X \rangle_E$ and $\langle X \rangle_C$. Results show both ends and centers behaved as $\langle X \rangle_{E \text{ or } C} \sim t^{1/4}$. The Rouse model predicts that the average monomer interpenetration depth for the entire chain scales with time to the one-quarter power as well. The ability for whole chain scaling to describe both the end and center sections behavior equally, at all times, is a characteristic signature of all isotropic friction models, e.g., Schweizer's polymer mode−mode coupling[12] or Ngai's coupling model.[27]

Rouse chain centers did not lag behind the ends in crossing the interface; they instead crossed the interface at all times (Figure 5a). This is directly caused by the isotropic nature of the segmental friction and is in contrast to the predictions of the reptation model. There a distinct lag in the mobility of Centers across the interface was observed due to anisotropic friction, as shown in the next section.
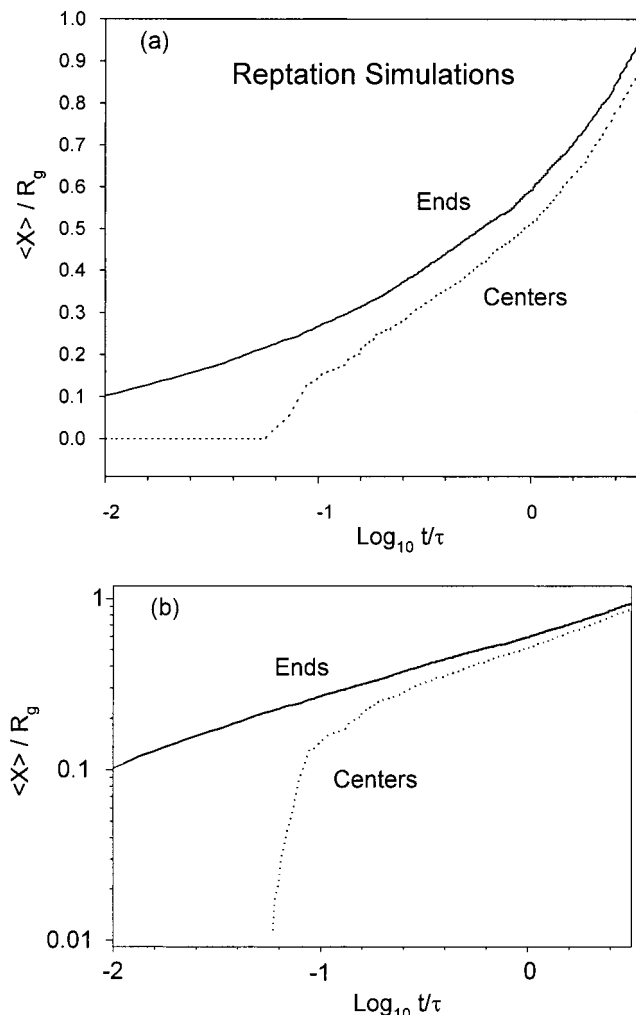
Figure 6. Reptation simulation predictions of average monomer interpenetration depth vs welding time for segments in the end ($\langle X \rangle_E$, solid curve) and center sections ($\langle X \rangle_C$, dotted curve) from computer simulations. Data are plotted on (a) linear–log axes and (b) log–log axes. In (a), $\langle X \rangle_E$ increases continuously, but $\langle X \rangle_C$ remains zero until a takeoff time, t_0, of about 0.1τ. In (b), ends show a slope of $1/4$ while centers show a highly time-dependent slope. This time-dependent slope is discussed in the text.

4.1.2. Reptation Simulations.
Reptation computer simulation predictions for the average interpenetration distance for segments in the chain end $\langle X \rangle_E$ and center sections $\langle X \rangle_C$ versus welding time are shown in Figure 6. The chain ends crossed the interface immediately, and $\langle X \rangle_E$ increased continuously (Figure 6a). From the log–log plot of these data (Figure 6b) ends behaved as $\langle X \rangle_E \sim t^{0.27}$. In contrast, Figure 6a shows that chain centers did not cross the interface immediately; instead they lagged until a takeoff time, t_0, of around 0.1τ ($\langle X \rangle_C = 0$ for $t < t_0$). The log–log plot slope of $\langle X \rangle_C$ (Figure 6b) clearly depends on welding time. This time dependence was consistent with the function

$$\langle X \rangle_C \sim (t - t_0)^\alpha \tag{13}$$

where α is the exponent. Equation 13 represents a shift in the time axis intercept of $\langle X \rangle_C$ to t_0. The slope of eq 13 when plotted in Figure 6b, $d(\log \langle X \rangle_C)/d(\log t)$, is α', written

$$\alpha' = \alpha \left[\frac{t/\tau}{t/\tau - t_0/\tau} \right] \tag{14}$$

Substituting the observed t_0 and $\alpha = 1/4$, the scaling exponent predicted by reptation dynamics, results in an α' of

$$\alpha' = 0.25 \left[\frac{t/\tau}{t/\tau - 0.1} \right] \tag{15}$$

Equation 15 closely matches the slope behavior seen for centers in Figure 6b. Thus, the time lag behavior of centers was understood, accounting for a shift of the time axis intercept of $\langle X \rangle_C$ from zero to t_0. The observed lag was a direct result of the anisotropic friction coefficient, created by the tube constraint of the reptation model, since centers must follow ends across the interface for snakelike motions. This lag behavior should be readily observable, if it exists, in the experiments.

At times longer than τ, centers showed interpenetration depth increasing like ends and all quantities approached $\langle X \rangle \sim t^{1/2}$. In addition to the dynamic behavior of the ends and centers, several static parameters can be evaluated. These are summarized as

$$\langle X(\tau) \rangle_E = 0.85 R_g$$
$$\langle X(\tau) \rangle_C = 0.77 R_g$$
$$\langle X(\tau) \rangle = 0.82 R_g \tag{16}$$

4.1.3. Minor Chain Reptation Calculations.
Figure 7 shows average interpenetration depths for segments in the end and center sections of the chain predicted by minor chain reptation model calculations. $\langle X \rangle_E$ increased immediately and continuously, while $\langle X \rangle_C$ remained at zero until a takeoff time, $t_0 \approx 0.7\tau$ (Figure 7a). The log–log plot of these data (Figure 7b) shows ends scaling as $\langle X \rangle_E \sim t^{1/4}$, consistent with the reptation prediction for the whole chain. Conversely, in Figure 7b, the $\langle X \rangle_C$ scaling depends on time, similar to reptation simulation results shown in Figure 6b. The apparent slope for centers was well described by eq 14, using $\alpha = 1/4$ and the observed $t_0/\tau \approx 0.5$ for minor chain calculations. The dynamic properties of the segments in the end section of the chain were then well described by the whole chain predictions of the reptation model. Chain centers in contrast showed a lag, characteristic of friction anisotropy. The static properties of minor chain calculations are summarized as

$$\langle X(\tau) \rangle_E = 0.43 R_g$$
$$\langle X(\tau) \rangle_C = 0.22 R_g$$
$$\langle X(\tau) \rangle = 0.40 R_g \tag{17}$$

4.2. End and Center Interdiffusion Experiments.
4.2.1. Depth Profiles.
Specular neutron reflectivity (SNR) was used to measure deuterium concentration profiles in HDH/dPS and HDH/hPS bilayer samples as a function of welding time for $t/\tau \le 1.5$. Figures 3 and 4 show representative reflectivity data (symbols) at two annealing times for ends (HDH/dPS) and centers (HDH/hPS) samples, respectively. Model reflectivity data, calculated using SERF, are shown in Figures 3 and 4 as solid curves through the experimental data. Scattering length density depth profiles ($\rho_b(z)$) used to calculate
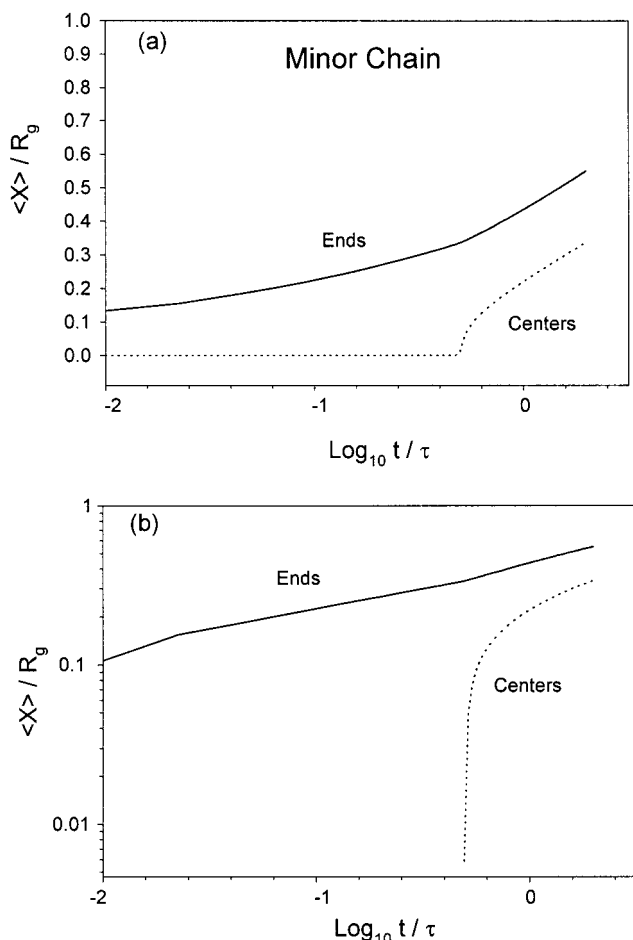
Figure 7. Minor chain reptation prediction of average inter-penetration depth vs welding time for segments in the chain end ($\langle X \rangle_E$) and center ($\langle X \rangle_C$) sections. Data are plotted on (a) linear−log axes and (b) log−log axes. In (a), segments in the end sections cross the interface continuously, while chain centers show a distinct lag until a takeoff time, $t_0 \approx 0.5\tau$. In (b), the ends show a constant slope while centers show a highly time-dependent slope, discussed in the text.

model reflectivities are shown in the inset plots of Figures 3 and 4.

SNR deuterium concentration profiles at representative welding times are presented in Figure 8. Figure 8a presents data for the ends case (HDH/dPS) with increasing welding time from top to bottom. Figure 8b presents data for the centers case (HDH/hPS) in the same fashion. The first two depth profiles in Figure 8, plots i, show data after a very brief welding ($t/\tau = 0.001$). A small broadening of the interface was evident in both samples, giving interface widths of less than 100 Å. This broadening indicated that segments move rapidly over short distances after brief welding. The commonality of plots i for the two samples indicated that this fast relaxation process occurred uniformly over the length of the chain at early times. This fast relaxation process is discussed in more detail later.

During further welding, up to $t/\tau = 0.13$, the behavior of the ends and centers diverged (Figure 8, plots ii). In this interval, the ends interface showed additional broadening, while the centers profile did not change. Significantly, no increase in interface breadth was seen for the centers sample. Figure 2a demonstrates the interface broadening process caused by end segments crossing the interface in the ends sample, an exchange of D for H. During the same time period, the centers

depth profile did *not* show additional broadening (Figure 8b, plots i and ii). It is clear that some portion of the chain was mobile during welding, but end section segments can cross the interface without altering the deuterium depth profile in the centers sample (HDH/hPS). This process is demonstrated in Figure 2b, where an even exchange of H for H occurs when end segments cross the interface. This produces no measurable change in the deuterium depth profile in the sample. The divergence of ends and centers depth profiles at these intermediate times indicated that while end segments are mobile, center segments are not crossing the interface.

Ends and centers depth profiles after welding for approximately one-quarter the relaxation time ($t/\tau = 0.23$) are plotted in Figure 8, plots iii. The broadening process continued in the ends sample. Here the centers depth profile began to show broadening beyond the early fast relaxation of plot i. This indicated that center segments have begun to cross the interface, as demonstrated in the last panel of Figure 2b. The initiation of interface broadening defines the centers takeoff time (t_0/τ); therefore, the observed takeoff is between 0.13τ and 0.23τ.

A simple argument can be used to estimate the reptation predicted takeoff time. The HDH chains used had a 25−50−25% length block structure. No center segments can cross the interface by strictly reptative motion until at least one-quarter of the chain has escaped the initial tube. Only a small fraction of chains will have center segments that cross the interface at this point, but the condition provides a lower limit for the takeoff time. Inserting this condition into eq 4 results in a reptation takeoff time estimate of

$$t_0 = 0.12\tau \tag{18}$$

This simple estimate is in good agreement with the experimental t_0, which was observed to be between 0.13τ and 0.23τ.

Plots iv of Figure 8 show deuterium depth profiles for ends and centers after welding beyond the relaxation time of the polymers. Beyond the relaxation time, ends and centers should behavior similarly, since here chain centers of mass have moved a distance greater than the radius of gyration and all correlation of ends and centers is lost. This is the behavior observed in Figure 8, plots iv.

We conclude that the behavior of the depth profiles in Figure 8 is very similar to the depth profiles sketched in Figure 2 for reptating chains. The depth profiles show strong qualitative evidence that center section segments followed behind end section segments, a signature of reptating chains.

4.2.2. Average Interpenetration Depth. To further compare these experimental data to the dynamics theory predictions presented in section 4.1, average monomer interpenetration depths ($\langle X(t) \rangle$) were calculated from experimental concentration depth profile data using eq 1. The results of these calculations ($\langle X \rangle_E$ and $\langle X \rangle_C$) are presented in Figure 9 as a function of the normalized welding time (t/τ).

4.2.2.1. Initial Broadening. Figure 9a indicates that, almost immediately after heating to $T > T_g$, both end and center interpenetration depths, $\langle X \rangle_E$ and $\langle X \rangle_C$, jumped to about 30 Å. This was driven by the depth profile broadening seen in Figure 8, plots i.
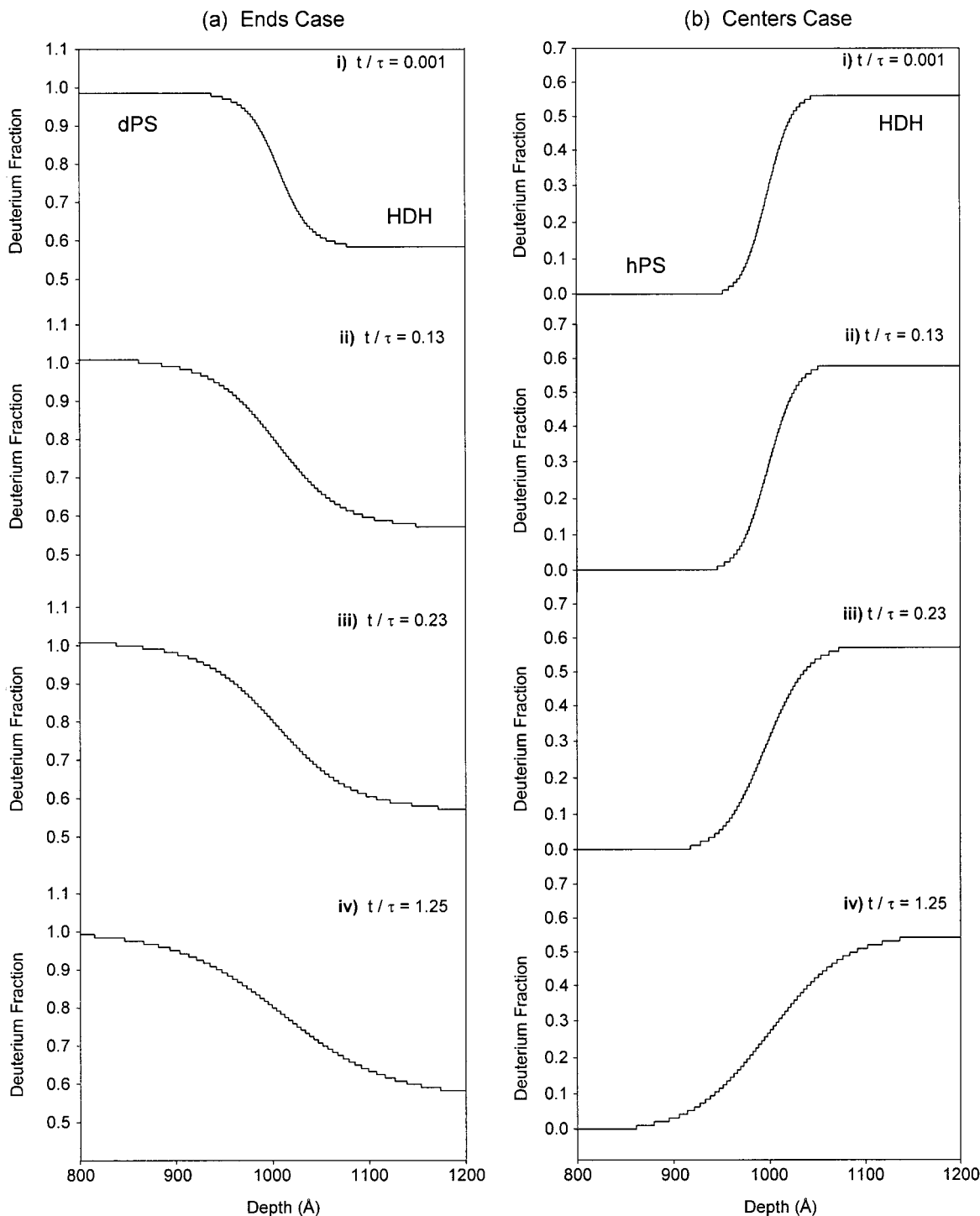
Figure 8. Deuterium fraction vs depth profiles at several welding times: (a) ends case and (b) centers case. Plots i show data at welding time of 0.001τ, where a small initial broadening was evident for both ends and centers. Plots ii show data at 0.13τ. An increase in interface broadening was seen for ends, while centers did *not* show significant additional broadening. Plots iii show data at 0.23τ. Ends showed continued broadening while the centers interface began to broaden. Plots iv show data at 1.25τ, which is beyond the relaxation time, where (a) and (b) show similar interface breadth. Detailed comparison of (a) and (b) and resulting dynamics implications are discussed in the text.

The distance between entanglements is approximated by the entanglement radius of gyration (R_{ge}), here approximately 47 Å using

$$R_{\text{ge}} = \left(\frac{C_\infty M_e j}{6 M_0}\right) b_0 \tag{19}$$

where C_∞ is the characteristic ratio, M_e the entanglement molecular weight ($\sim$18K for PS), M_0 the repeat

unit molecular weight, j the bonds per repeat unit, and b_0 the repeat unit length. Segmental motions over distances less than R_{ge} will not be affected by neighboring chains, and a Rouse relaxation process is expected on this length scale. The relaxation time of this process, τ_e, is 0.001τ.

The welding time in Figure 8, plots i, is coincident with τ_e, and the observed relaxation length scale is consistent with Rouse segmental motions between
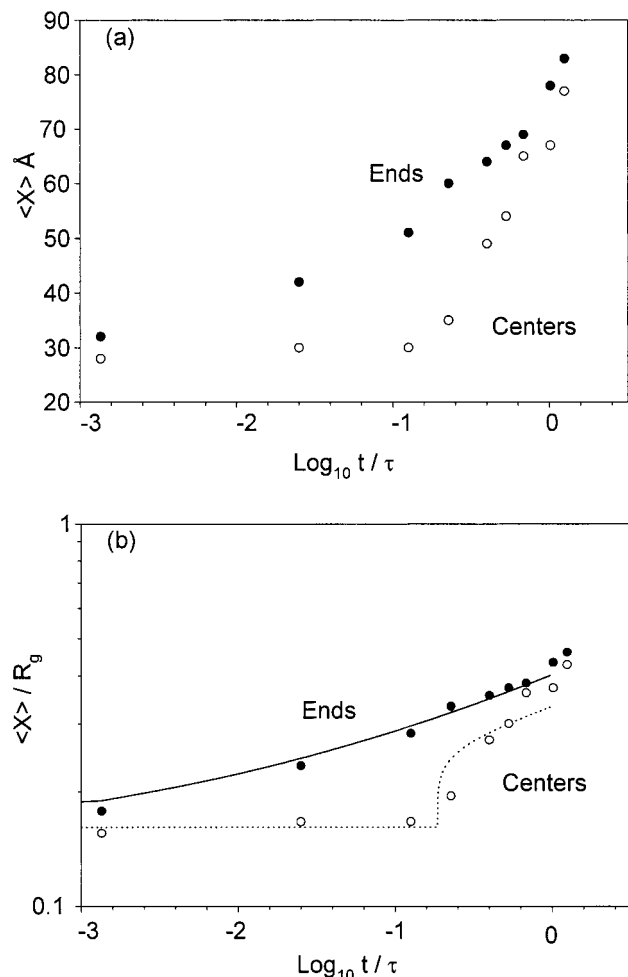
Figure 9. Specular neutron reflectivity derived average interpenetration depth vs welding time data for chain end ($\langle X \rangle_E$, solid symbols/curve) and center ($\langle X \rangle_C$, open symbols/dotted curve) sections. Data are plotted on linear−log axes in (a) and on log−log axes in (b). In (a), segments in the end sections cross the interface continuously, while chain centers show a distinct lag until a takeoff time $t_0 \approx 0.15\tau$. In (b), the ends show a constant slope up to $t/\tau \approx 1$ and centers show a time-dependent slope, as discussed in the text.

entanglements. Rouse relaxation between entanglements would also affect all sections of the chain equally, again consistent with the observed similarity of ends and centers data in plots i of Figure 8.

This "bursting" phenomenon was seen previously in polymer interdiffusion experiments.[28,29] Alternative interpretations have been suggested and include nonequilibrium initial structure relaxing quickly upon heating above T_g, differences in mobility of the surface layer compared to the bulk, and relaxation of surface tension between layers. The observed rapid broadening at early times may then be a result of one or more physical processes, but Rouse relaxation between entanglements is consistent with these results.

4.2.2.2. Lag of Center Segments. The intermediate time regime of Figure 9a ($-3 < \log t/\tau < -1/2$) showed the most interesting features. After the initial broadening, $\langle X \rangle_C$ remained constant for better than 2 decades of normalized welding time. During this same interval, $\langle X \rangle_E$ increased continuously. This lag in centers mobility, while ends showed continuous mobility, is a characteristic signature of reptation. The takeoff time (t_0), determined by motions greater than 30 Å, was ap-

proximately 0.15τ. This falls between the predictions of reptation simulations and minor chain reptation calculations.

4.2.2.3. Scaling Exponents of Ends and Centers. Scaling exponents for the average interpenetration depth of ends and centers were extracted from experimental data by log $\langle X \rangle$ versus log t analysis, shown in Figure 9b. After the rapid increase, ends data showed a slope that smoothly increased to one-quarter with welding. Beyond the relaxation time, the slope increased sharply, tending toward $t^{1/2}$.

The slope of the centers data in Figure 9b clearly changed with welding time. The slope was fit well by the α' expression of eq 14 using $\alpha = 1/4$ and $t_0/\tau = 0.15$. These $\langle X \rangle_C$ data clearly show a nonzero takeoff time t_0, indicating a shift of the time axis intercept. This behavior is characteristic of reptation dynamics as shown by simulations and minor chain calculations. The scaling analysis results are summarized as

$$\langle X \rangle_E \sim t^{1/4} \quad \text{for } t < \tau$$

$$\langle X \rangle_C \sim t^0 \quad \text{for } t < t_0$$

$$\langle X \rangle_C \sim t^{\alpha'} \quad \text{for } 2t_0 < t < \tau \quad (20)$$

where α' is the apparent slope from eq 14 with $\alpha = 1/4$ and $t_0/\tau = 0.15$.

The static behavior of the experiments are summarized as

$$\langle X(\tau) \rangle_E = 0.43 R_g$$

$$\langle X(\tau) \rangle_C = 0.37 R_g \quad (21)$$

which compare well with minor chain calculation results.

4.2.2.4. Whole Chain Results. Average monomer interpenetration depth, $\langle X \rangle$, results have been compared to theoretical predictions for the mean-square segment displacement, X, in the literature.[28−31] However, these two properties are defined using different reference states and therefore are not expected to be identical. The difference in definition leads to different behavior predictions for a single dynamics model, especially at early times.

A polymer chain segment, j, currently at position $\mathbf{R}_j(t)$, was at position $\mathbf{R}_j(0)$ initially. The displacement of segment j at time t is simply the difference between these positions. The root-mean-square segment displacement for a chain is the average displacement over all N segments, written

$$X(t) = \sqrt{\langle X^2(t) \rangle} = \langle [\mathbf{R}_j(t) - \mathbf{R}_j(0)]^2 \rangle^{1/2} \quad (22)$$

Doi and Edwards have described the predicted behavior of $X(t)$ for the reptation model.[11] At early times the segments move within the tube and are not constrained by entanglements. When displacements reach the tube diameter, the segments begin to be constrained by the tube. The time of this crossover is defined as the entanglement relaxation time, τ_e, and for times less than τ_e the scaling is predicted as $X \sim t^{1/4}$. After τ_e, displacements are restricted to the reptation process, subject to two remaining relaxation times. For motions up to the Rouse relaxation time, τ_{RO}, the scaling is predicted to scale as $X \sim t^{1/8}$. Beyond τ_{RO}, but less than the
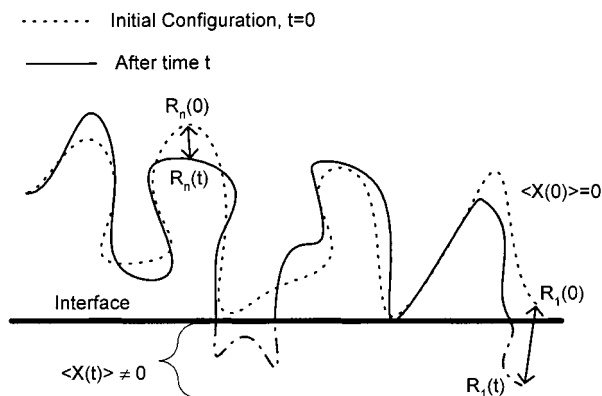
**Figure 10.** A polymer chain at time zero, dotted, and time t, solid curve. The positions of segments 1 and n at both times are indicated. $X(t)$ is an average of all segment displacements, regardless of position relative to the interface plane. Segments that have crossed the interface plane at time t are shown by the dot–dash curve. Only these segments are included in the calculation of $\langle X(t) \rangle$. The behavior of $X(t)$ and $\langle X(t) \rangle$ at early times is expected to differ on the basis of this definition difference, even for a single dynamics model.

reptation relaxation time, τ_d, the scaling is predicted as $X \sim t^{1/4}$, and for times beyond τ_d the scaling is predicted as $X \sim t^{1/2}$.[11]

The average monomer interpenetration depth for the entire chain, $\langle X \rangle$, is a measure of the distance segments have traveled beyond a *fixed* interface plane. The calculation of $\langle X \rangle$ then includes only segments that have crossed the interface plane. The definitions of $X(t)$ and $\langle X(t) \rangle$ are sketched in Figure 10. At time zero, there are no segments beyond the interface plane and $\langle X(0) \rangle = 0$. As interdiffusion proceeds, the number of segments that have crossed through the plane increases. At time t, M segments, shown as dot–dash curve in Figure 10, have crossed the interface, and their distance from the interface at time t is included in $\langle X(t) \rangle$. At some later time, $t + \Delta t$, ΔM additional segments have crossed the interface. Therefore, $\langle X(t+\Delta t) \rangle$ is the average position calculated for $M + \Delta M$ segments, which is larger than the number of segments included in $\langle X(t) \rangle$. In the same time interval, Δt, the original M segments may have moved farther from the interface plane, but the net change in $\langle X \rangle$ is a balance of the increase in the sum of the positions (numerator) and an increase in the number of segments (denominator). $\langle X \rangle$ uses a fixed plane in space as a reference state, not the initial conformation of the chain, leading to different scaling predictions for $\langle X \rangle$ compared to X, especially at early times.

At early times, $\langle X \rangle$ is expected to increase rapidly since the averaging process excludes segments that move away from the interface and those that have not moved significantly from their initial coordinates. $\langle X \rangle$ then jumps sharply at early times, on the order of τ_e. This early increase continues to affect the observed behavior of $\langle X \rangle$ for times much beyond τ_e. As welding proceeds, more segments cross the interface, reducing the effect on $\langle X \rangle$ of the segments at the outer edge of the interdiffusion front. $\langle X \rangle$ then represents a balance between the early time motions and the onset of slower long-range diffusion. Assuming these longer-range motions occur by reptation, we expect that $\langle X \rangle$ scales with time more weakly than X since it has increased so sharply at earlier times. Beyond τ_{RO}, we expect $\langle X \rangle$ to scale with time to a power less than $^1/_4$. As reptation begins to dominate $\langle X \rangle$, the effect of the interface is
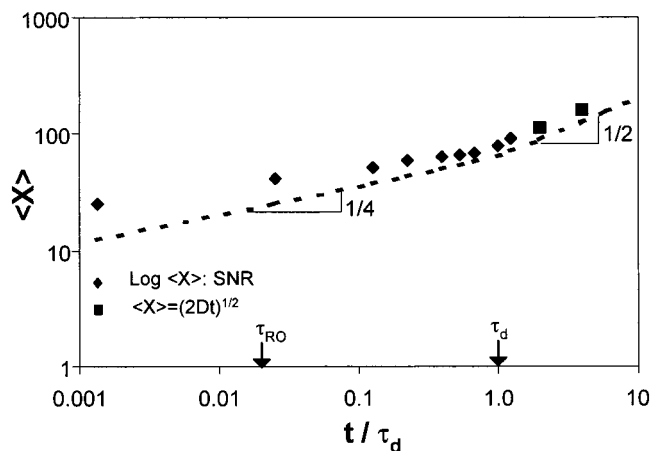
Figure 11. Whole chain average interpenetration depth plotted versus normalized welding time on log–log axes. Diamonds show data derived from SNR concentration profiles, and squares represent data estimated by $\langle X \rangle = (2Dt)^{1/2}$ at long times. Slope lines of one-quarter and one-half are shown for comparison.

weaker, and the behavior of $\langle X \rangle$ is expected to approach that of X. Thus, early on $\langle X \rangle$ and X differ, but as the longest relaxation time is approached, the two predictions are expected to converge.

Whole chain $\langle X \rangle$ data were derived from our experiments and are plotted in Figure 11. Slope lines of one-quarter and one-half are also plotted for reference. The data showed a slope less than one-quarter for times up to and beyond τ_{RO}. Between τ_{RO} and τ_d, the slope increased to one-quarter. Beyond τ_d, $\langle X \rangle \sim t^{1/2}$. These results are consistent with the reptation expectations for $\langle X \rangle$ scaling described above.

The purpose of this section is to point out a commonly overlooked feature of the definition of $\langle X \rangle$. Direct comparison of $\langle X \rangle$ measured via interdiffusion experiments and X predictions made by bulk dynamics theories is problematic since the predictions of the two properties differ for a single dynamics model. Considering the interfacial character of $\langle X \rangle$, agreement between reptation predicted behavior of $\langle X \rangle$ and our experiments is evident.

5. Conclusions

The motions of segments in the center and end sections of polymer chains were monitored via the deuterium depth profiles of two welding couples: triblock polymer chains (HDH) with either fully deuterated (dPS) or protonated polymer (hPS). The behaviors of segments in the chain end and center sections were monitored directly via deuterium depth profiles using specular neutron reflectivity. Rouse and reptation dynamics predictions were developed using computer simulations and numerical calculations. These models are representative of two important classes of dynamics theories: isotropic friction and anisotropic friction, respectively.

The experimental results presented herein were consistent both qualitatively and quantitatively with the predictions of the reptation model and were in stark contrast to Rouse predictions. Specifically, a distinct lag in the mobility of segments in the center section across the interface was observed in experiments and in reptation simulations and minor chain calculations. This lag is a highly characteristic signature of anisotropic friction, caused by entanglement constraints. Models

using isotropic friction (Rouse, PMC, etc.) do not predict a lag for centers. This paper has also presented a detailed analysis of the lag behavior, including its effect on the log–log scaling of average interpenetration depths. The observed takeoff time ($0.13 < t_0/\tau < 0.23$) fell between reptation simulation and minor chain reptation predictions, in reasonable agreement with both. The ability of eqs 13 and 14 to describe the behavior of both experiments and reptation predictions provided strong evidence that the observed behavior is consistent with reptation dynamics.

The reptation model and its descendants are thus capable of explaining these results. Isotropic friction models such as Rouse and PMC are not capable of describing these data. Combined with the "ripple" results presented previously, the evidence is very clear that reptation provides an extremely accurate description of the behavior of melt polymer chains near weld interfaces.[6]

References and Notes

(1) Wool, R. P. *Polymer Interfaces: Structure and Strength*; Hanser Publishers: Munich, 1995.
(2) Green, P. F.; Kramer, E. J. *Macromolecules* **1986**, *19*, 1108.
(3) Summerfield, G. C.; Ullman, R. *Macromolecules* **1987**, *20*, 401.
(4) Tirrell, M. *Rubber Chem. Technol.* **1984**, *57*, 523.
(5) Klein, J.; Briscoe, B. J. *Proc. R. Soc. London A* **1979**, *365*, 53.
(6) Welp, K. A.; Wool, R. P.; Satija, S. K.; Pispas, S.; Mays, J. *Macromolecules* **1998**, *31*, 4915.
(7) Russell, T. P.; Deline, V. R.; Dozier, W. D.; Felcher, G. P.; Agrawal, G.; Wool, R. P.; Mays, J. W. *Nature* **1993**, *365*, 235.
(8) Agrawal, G.; Wool, R. P.; Dozier, W. D.; Felcher, G. P.; Russell, T. P.; Mays, J. W. *Macromolecules* **1994**, *27*, 4407.
(9) Agrawal, G.; Wool, R. P.; Dozier, W. D.; Felcher, G. P.; Zhou, J.; Pispas, S.; Mays, J. W.; Russell, T. P. *J. Polym. Sci., Part B* **1996**, *34*, 2919.
(10) de Gennes, P. G. *J. Chem. Phys.* **1971**, *55*, 572.
(11) Doi, M.; Edwards, S. F. *The Theory of Polymer Dynamics*; Oxford University Press: New York, 1986.
(12) Schweizer, K. S. *J. Chem. Phys.* **1989**, *91*, 5802, 5822.
(13) Rouse, P. E. *J. Chem. Phys.* **1953**, *21*, 1272.
(14) Zhao, W.; Zhao, X.; Rafailovich, M. H.; Sokolov, J.; Composto, R. J.; Smith, S. D.; Satkwoski, M.; Russell, T. P.; Dozier, W. D.; Mansfield, T. *Macromolecules* **1993**, *26*, 561.
(15) Botelho do Rego, A. M.; Lopes da Silva, J. D.; Rei Vilar, M.; Schott, M.; Petitjean, S.; Jerome, R. *Macromolecules* **1993**, *26*, 4986.
(16) Welp, K. A.; Wool, R. P., work in progress.
(17) Kim, Y. H.; Wool, R. P. *Macromolecules* **1983**, *16*, 1115.
(18) Zhang, H.; Wool, R. P. *Macromolecules* **1989**, *22*, 3018.
(19) Agrawal, G. A. Ph.D., University of Illinois, 1994.
(20) Tassin, J. F.; Monnerie, L.; Fetters, L. J. *Macromolecules* **1988**, *21*, 2404.
(21) Russell, T. P. The Characterization of Polymer Interfaces. *Annu. Rev. Mater. Sci.* **1991**, *21*, 249.
(22) Lekner, J. *Physica B* **1991**, *173* (1–2), 99.
(23) Majkrzak, C. F. In *Neutron Scattering in Materials Science II*; Neumann, D. A., Russell, T. P., Wuensch, B. J., Eds.; Materials Research Society: Pittsburgh, 1995; Vol. 376, p 143.
(24) Bouchaud, E.; Farnoux, B.; Sun, X.; Daoud, M.; Jannink, G. *Europhys. Lett.* **1986**, *2*, 315.
(25) Stamm, M. In *Physics of Polymer Surfaces and Interfaces*; Sanchez, I. C., Ed.; Butterworth-Heinemann: Boston, 1992; p 163.
(26) Welp, K. A.; Co, C. C.; Wool, R. P. *J. Neutron Res.,* in press.
(27) Ngai, K. L. *Comments Solid State Phys.* **1979**, *9*, 1651.
(28) Karim, A.; Mansour, A.; Felcher, G. P.; Russell, T. P. *Phys. Rev. B* **1990**, *42*, 6846.
(29) Stamm, M.; Huttenbach, S.; Reiter, G.; Springer, T. *Europhys. Lett.* **1991**, *14*, 451.
(30) Karim, A.; Felcher, G. P.; Russell, T. P. *Macromolecules* **1994**, *27*, 6973.
(31) Kunz, K.; Stamm, M. *Macromolecules* **1996**, *29*, 2548.